Nucleon-Nucleon Scattering*†

HERMAN FESHBACH, *Department of Physics and Laboratory for Nuclear Science, Massachusetts Institute of Technology, Cambridge, Massachusetts*

AND

EARLE LOMON, *Weizmann Institute of Science, Rehovoth, Israel*

(Received November 21, 1955)

Nucleon-nucleon scattering data from 0 to 274 Mev are discussed by means of a boundary-condition approximation. For internucleon distances greater than the core radius, which may depend on the state under discussion, the nucleon-nucleon interaction is assumed to vanish, while at the core radius the logarithmic derivative of the wave function or the reaction matrix satisfies a boundary condition. Assuming charge independence, it has been found possible to fit most of the experimental data with all but one boundary condition energy-independent. The core radius for the $^1S_0$ state is assumed to decrease with increasing energy. We find that $p-p$ scattering is composed mostly of scattering in the $^1S_0$ and $^3P_0$ states, both of which give isotropic distributions. The scattering from the $^3P_0$ state is close to the scattering by a repulsive sphere of radius 1.32×10^{-13} cm. The scattering in the isotopic singlet state below 100 Mev, assuming that the $n-p$ angular distribution is symmetric about 90°, is entirely determined by the low-energy fit to triplet $(^3S_1+^3D_1)$ $n-p$ scattering. Above 100 Mev the $(^3S_1+^3D_1)$ states make the major contribution to the isotopic singlet scattering. The predicted cross sections fail significantly in only one detail: they are not sufficiently large for $n-p$ scattering near 180°. Regardless of the validity of this particular fit, the boundary-condition approximation is found to provide a comparatively simple method for the broad correlation and understanding of the experimental results.

I. INTRODUCTION

MOST of the various phenomenological models which have been suggested for the correlation of nucleon-nucleon scattering data assume a local potential $V(\mathbf{r},\boldsymbol{\sigma},\boldsymbol{\tau})$ between the nucleons.[1] Here $\mathbf{r}$ is the internucleon radius vector, $\boldsymbol{\sigma}$ represents the spin operators for each nucleon and $\boldsymbol{\tau}$ the isotopic spin. These models have become more and more complex as more data have become available, but nevertheless have failed to match the experiments in one or more crucial aspects. The most successful of these models, the one proposed by Jastrow,[2] does remarkably well in fitting angular distributions as well as total cross sections, but fails to yield appropriate polarizations as well as sufficient isotropy for $p-p$ scattering.[3]

On the other hand, developments in the meson theory of nuclear forces[4] suggest that such a simplified description of nuclear forces is only possible if the two nucleons are far apart. When r is less than the meson Compton wavelength, higher order effects, in which many mesons are interchanged, become important, and a nonlocal potential is required to describe the nucleon-nucleon interaction. This region is, of course, very important in high-energy nucleon-nucleon scattering.

In the present paper, we shall go to the extreme of using a completely nonlocal interaction. Specifically, the interaction in each state is to be represented by a boundary condition on the logarithmic derivative of the wave function at a core of radius r_0, which may depend on the state in question. In other words, we shall determine the reaction matrix for the system. For r greater than r_0, the interaction energy will be taken to vanish. Such a description was employed by Breit and Bouricius[5] for the discussion of low-energy singlet S scattering. Here we shall generalize so as to include triplet scattering with tensor mixing as well as states of angular momentum higher than zero. The boundary conditions are clearly equivalent to the phase shifts and are, therefore, just another representation of the data. However, as we shall find, the boundary conditions we obtain are mainly independent of the energy. This result has definite implications for the physical nature of the nucleon-nucleon interaction, implications which we shall now discuss. Of course, it should be borne in mind that a boundary-condition model is at best a rough approximation to the actual interaction.

One of the implications of the meson theory of nuclear forces is its indication of a region in which many virtual mesons are present, or equivalently in which the interaction energy is large. Here the behavior of the nucleons will be relatively insensitive to the value of their kinetic energy at infinity. Of course, this region has no sharp boundary. Rather one can only say that such an energy-independent description will hold accurately for sufficiently small interparticle distances. One would expect that, as the kinetic energy at infinity increases, the region in which an energy-independent description remains possible will shrink. For large internucleon distances the interaction energy according to meson theory should be described by a

* Supported in part by the joint program of the U. S. Atomic Energy Commission and the Office of Naval Research.

† Presented in part at the Washington meeting of the American Physical Society, 1953; Phys. Rev. **91**, 454(A) (1953).

[1] See for example R. S. Christian and E. W. Hart, Phys. Rev. **77**, 443 (1950); and R. S. Christian and H. P. Noyes, Phys. Rev. **79**, 85 (1950).

[2] R. Jastrow, Phys. Rev. **79**, 389 (1950); **81**, 165 (1951).

[3] L. J. B. Goldfard and D. Feldman, Phys. Rev. **88**, 1099 (1952); D. Swanson, Phys. Rev. **89**, 740 (1953); **89**, 749 (1953).

[4] M. M. Levy, Phys. Rev. **88**, 725 (1952); A. Klein, Phys. Rev. **90**, 1101 (1953); **92**, 1017 (1953); S. Drell and K. Huang, Phys. Rev. **91**, 1527 (1953).

[5] G. Breit and W. G. Bouricius, Phys. Rev. **75**, 1029 (1949).

local potential insofar as the "low-energy" theorems are valid.

This suggests the following phenomenological model. We crudely represent the energy-independent core by means of a set of energy-independent boundary conditions at a core distance r_0, which may be state dependent. For $r>r_0$ we would then assume phenomenological local potentials. Levy's and Jastrow's models fall into this general class, for they took a repulsive core corresponding to the wave function going to zero at the boundary of the core. As the kinetic energy increases, we would expect r_0 to shrink with energy (or equivalently the boundary conditions would change). These changes should be quite small for energies considerably less than the average interaction energy in the core, i.e., for several hundred Mev.

We now compare this description with the one actually used in this paper, in which the local potentials external to the core are dropped. We shall refer to the latter as the boundary-condition approximation.[6] One would expect that this approximation will be more energy dependent than those describing the more refined model. In particular, at low energies the core radius should, in order to include the effect of external potentials, be of the order of the meson Compton wavelength and thus considerably larger than the actual core radius. As the energy increases, the core radius should shrink until at sufficiently high energies, where the external potentials are not important, it should approach the correct core radius.[7]

We conclude the introduction by indicating this paper's scope and limitations and by summarizing its contents. We shall attempt to fit all nucleon-nucleon scattering data in the energy range from 0 to 274 Mev. This fit should not be expected to be precise, since small deviations might very well be accounted for by corresponding fluctuations in the boundary conditions. Our main objective will be to obtain a broad correlation and understanding of the data. It is just for this purpose that the boundary-condition approximation is most useful, and this should be regarded as one of our principal results independent of the validity of the particular fit of the data we obtain. Calculations with this approximation are very much simpler than those required by a potential model but still, as we have seen, rather direct physical interpretation of the results may be obtained.

The contents of the paper are as follows. In Sec. II the formal analysis of the problem is presented. We include here the explicit formulas (1) for the phase shifts including low-energy effective range approximation; (2) for binding energy of the bound states; (3) differential and total cross sections; and (4) for polarization. In Sec. III, the low-energy data ($p-p$ scattering, $n-p$ scattering and properties of the deuteron) are discussed. In Sec. IV we turn to the high-energy data. Section V contains the conclusion and, in particular, a list of the boundary parameters required to fit the data.

[6] Another insight into the boundary-condition approximation may be obtained if one notes its equivalence to an infinitely repulsive well for $r<r_0$ and a singular potential at $r=r_0$. In effect, then, this approximation compresses the external potential such as that given by Levy or Jastrow into the singular potential.

[7] It should be noted that the scattering resulting from the usual monotonic potentials can be represented by an energy-dependent boundary condition. Such energy dependence would usually be more rapid than that described here and would even require, at some energies, negative core radii.

II. FORMAL ANALYSIS

The fundamental assumption of our model is expressed in terms of a boundary condition

$$r_0(d\Psi/dr)_{r=r_0}=F\Psi(r_0), \tag{1}$$

where Ψ is a state or appropriate group of states of the same total angular momentum, r_0 is the core radius assigned to Ψ. For the singlet states

$$\Psi=\psi_l, \tag{2}$$

where l is the orbital angular momentum in units of $\hbar$. The corresponding core radius is r_{0l}, and the boundary parameter F is f_l. A similar simple structure prevails for the triplet states in which J, the total angular momentum, equals l. The wave function is ψ_{JJ}, the core radius r_{0JJ}, the boundary parameter F is f_{JJ}. The other triplet states in which $l=J\pm1$ can couple so that Ψ is a unicolumnar matrix

$$\Psi=[\Psi_{J,l}]=\begin{bmatrix}\psi_{J,J-1}\\ \\ \psi_{J,J+1}\end{bmatrix}. \tag{3}$$

The corresponding core radius is written r_{0J}. F is an Hermitian matrix which we may take to be real since the complex parts of the elements of F may be absorbed into the wave function. F is given by

$$F_J=\begin{bmatrix}f_{J,J-1} & f_J^{(t)}\\ f_J^{(t)} & f_{J,J+1}\end{bmatrix}. \tag{4}$$

For example, F_1 will couple the $^3S_1$ and the $^3D_1$ states. The general form (4) breaks down for the $J=0$ triplet state, where only one state, the $^3P_0$, can enter. The core radius is r_{00} and the boundary parameter, f_{01}.

In the discussion below we shall usually drop the subscripts in r_0 designating the state since the latter will usually be stated explicitly.

Singlet Phase Shifts

For $r>r_{0l}$ the wave function ψ_l for the singlet state for the neutron-proton system is

$$\psi_l=A_l[h_l^{(2)}(x)+e^{2i\eta_l}h_l^{(1)}(x)], \tag{5}$$

where A_l is simply an amplitude, k is the relative wave number, $h_l^{(1)}(x)$ and $h_l^{(2)}(x)$ are spherical Hankel functions of the first and second kind:

$$\begin{aligned} h_l^{(1)}(x)&\longrightarrow(1/x)e^{i(x-\frac{1}{2}l\pi)} \quad \text{as} \quad x\longrightarrow\infty,\\ h_l^{(2)}(x)&\longrightarrow(1/x)e^{-i(x-\frac{1}{2}l\pi)} \quad \text{as} \quad x\longrightarrow\infty. \end{aligned} \tag{6}$$

The quantity η_l is the phase shift. Substituting form (5) into (1) leads immediately to an expression for the phase shift

$$\tan\eta_l = -\tan\delta_l \frac{f_l+\tan\alpha_l}{f_l+\tan\beta_l}, \tag{7}$$

where in terms of j_l and n_l, the spherical Bessel and Neumann functions,

$$\tan\delta_l = -(j_l/n_l); \quad \tan\alpha_l = -x_0(dj_l/dx)/j_l; \quad \tan\beta_l = -x_0(dn_l/dx)/n_l. \tag{8}$$

These functions are evaluated at $x_0=kr_0$.[8]

At low energies, particularly, it is useful to obtain explicit energy expansions of Eq. (7), which can be interpreted in terms of effective range and scattering length. We find for $l=0$ that

$$x_0\cot\eta_0 \simeq -\frac{f_0+1}{f_0}+\left[-\frac{1}{f_0}+\frac{f_0+1}{3f_0^2}\right]x_0^2 + \left[-\frac{1}{3f_0}+\frac{f_0+1}{3f_0^2}+\frac{(f_0+1)^2}{3f_0^2}\left(\frac{2}{5}-\frac{f_0+1}{3f_0}\right)\right]x_0^4 \simeq -r_0/a_0+\tfrac{1}{2}(\rho_0/r_0)x_0^2-P_0(\rho_0/r_0)^3x_0^4. \tag{9}$$

Hence, the scattering length a_0 and effective range ρ_0 are given by

$$a_0 = r_0 f_0/(f_0+1), \tag{10}$$

$$\rho_0 = 2r_0\left[\frac{(f_0+1)^2}{3f_0^2}-\frac{1}{f_0}\right]. \tag{11}$$

Similar expansions may be obtained for other l values:

$$\frac{x_0^{2l+1}}{(1\cdot3\cdot5\cdots2l+1)(1\cdot1\cdot3\cdots2l-1)}\cot\eta_l \simeq -\frac{(f_l+l+1)}{f_l-l} \times\left[1+x_0^2\left(\frac{2l+1}{(2l-1)(2l+3)}-\frac{1}{(f_l+l+1)(2l-1)}-\frac{1}{(f_l-l)(2l+3)}\right)\right]. \tag{12}$$

We turn now to singlet $p-p$ scattering. The main change from the $n-p$ analysis is that in (7) one must replace the spherical Hankel functions by the corresponding Coulomb wave functions. We shall not detail the results here as they will not be essential for much of our analysis. However, at low energies the analog of expansion (9) is required. This may be obtained from the work of Breit and Bouricius.[9] Making the appropriate expansions we find

$$(C_0^2/\eta)\cot\eta_0 - 2\ln\eta + q_0/\eta \simeq f^{(0)}+f^{(1)}/\eta^2+f^{(2)}/\eta^4. \tag{13}$$

Here

$$\eta = e^2/\hbar v, \quad \eta^{-2}=40.01E, \qquad C_0^2 = 2\pi\eta/(e^{2\pi\eta}-1), \quad q_0/2\eta = 2\gamma-1+\mathrm{Re}\psi(i\eta), \tag{14}$$

where γ is the Euler-Mascheroni constant, ψ is the logarithmic derivative of the gamma function, E is the energy in Mev in the laboratory system. The expressions for $f^{(i)}$ are

$$\begin{aligned} f^{(0)} &= -2\ln(2r_0/a)+(\alpha/\gamma),\\ f^{(1)} &= [(\beta/\gamma)-(\alpha\delta/\gamma^2)(r_0/a)](r_0/a),\\ f^{(2)} &= [(\epsilon/\gamma)-(\beta\delta/\gamma^2)](r_0/a)^3,\\ \alpha &= 2-4(r_0/a)-(f_0+1)(a/r_0), \quad \beta=\tfrac{1}{2}(f_0-1),\\ \gamma &= f_0-2(r_0/a), \quad \epsilon=\tfrac{1}{8}-f_0/24,\\ \delta &= (f_0/6)+\tfrac{2}{3}+(4/9)(r_0/a). \end{aligned} \tag{15}$$

The quantity a is $(\hbar^2/\mu e^2)$, where μ is the reduced mass of the proton-proton system; a equals 5.76×10^{-12} cm. The evaluation of $f^{(i)}$ is correct to order $(r_0/a)^3$.

Triplet Phase Shifts

The states for which $l=J$ are not coupled with the other triplet states. Hence, the phase shifts for these states are determined by the equations given above if we replace η_l by η_{JJ} and f_l by f_{JJ}. For the other states of a given J, $l=J\pm1$, the determining boundary conditions are

$$r_0\begin{pmatrix}\psi_{J,J-1}'\\ \psi_{J,J+1}'\end{pmatrix} = \begin{pmatrix}f_{J,J-1} & f_J^{(t)}\\ f_J^{(t)} & f_{J,J+1}\end{pmatrix}\begin{pmatrix}\psi_{J,J-1}\\ \psi_{J,J+1}\end{pmatrix}. \tag{16}$$

The wave functions and their derivatives are evaluated at $r=r_0$.

We shall only need to determine the "eigenscattering" mixtures and the corresponding eigenphases.[10] Let the eigenvector solutions of Eq. (16) be denoted by $\Phi_J^{(\alpha)}$, where α has two possible values, and the corresponding phase shifts are $\eta_J^{(\alpha)}$. Let

$$\Phi_J^{(\alpha)} = \begin{pmatrix}\varphi_{J,J-1}^{(\alpha)}\\ \varphi_{J,J+1}^{(\alpha)}\end{pmatrix}.$$

Then

$$\begin{aligned} \varphi_{J,J-1}^{(\alpha)} &= A_J^{(\alpha)}(j_{J-1}-\tan\eta_J^{(\alpha)}n_{J-1}),\\ \varphi_{J,J+1}^{(\alpha)} &= B_J^{(\alpha)}(j_{J+1}-\tan\eta_J^{(\alpha)}n_{J+1}), \end{aligned} \tag{17}$$

[8] Lowan, Morse, Feshbach and Lax, AMP Report 6.21R, Section 6.1–Sr 1046–2032 (unpublished).

[9] G. Breit and M. H. Hull, Jr., Am. J. Phys. **21**, 184 (1953); G. Breit, Revs. Modern Phys. **23**, 238 (1951).

[10] J. Schwinger (unpublished). J. Blatt and L. C. Biedenharn, Phys. Rev, **86**, 399 (1952).

where n_l is the spherical Neumann function. Substitution of (17) in (16) leads to a pair of linear homogeneous equations for $A_J^{(\alpha)}$ and $B_J^{(\alpha)}$. The determinant of the coefficients which must vanish leads to a quadratic equation determining $\tan\eta_J^{(\alpha)}$:

$$x_0[j_{J-1}'-(\tan\eta_J^{(\alpha)})n_{J-1}']=[j_{J-1}-(\tan\eta_J^{(\alpha)})n_{J-1}]$$
$$\times\left[f_{J,J-1}+\frac{(f_J^{(t)})^2}{\dfrac{x_0 j_{J+1}'-(\tan\eta_J^{(\alpha)})n_{J+1}'}{j_{J+1}-(\tan\eta_J^{(\alpha)})n_{J+1}}-f_{J,J+1}}\right]. \quad (18)$$

For greater convenience in discussing our results, we introduce the auxiliary quantity $F_J^{(\alpha)}$, which might be described as the effective diagonal coupling for the $l=J-1$ state, i.e.,

$$\tan\eta_J^{(\alpha)}=-\tan\delta_{J-1}\frac{F_J^{(\alpha)}+\tan\alpha_{J-1}}{F_J^{(\alpha)}+\tan\beta_{J-1}}, \quad (19)$$

in complete analogy to Eq. (7). From Eq. (18) $F_J^{(\alpha)}$ is the solution of the following quadratic equation

$$a(F_J^{(\alpha)})^2+bF_J^{(\alpha)}+c=0,$$

$$a=\tan\delta_{J-1}+\tan\eta_{J,J+1},$$

$$b=-f_{J,J-1}(\tan\delta_{J-1}+\tan\eta_{J,J+1})$$
$$+\tan\alpha_{J-1}\tan\delta_{J-1}+\tan\beta_{J-1}\tan\eta_{J,J+1}$$
$$+(f_J^{(t)})^2\frac{\tan\delta_{J-1}-\tan\delta_{J+1}}{f_{J,J+1}+\tan\beta_{J+1}}, \quad (20)$$

$$c=-f_{J,J-1}[\tan\alpha_{J-1}\tan\delta_{J-1}+\tan\beta_{J-1}\tan\eta_{J,J+1}]$$
$$+(f_J^{(t)})^2\frac{\tan\alpha_{J-1}\tan\delta_{J-1}-\tan\beta_{J-1}\tan\delta_{J+1}}{f_{J,J+1}+\tan\beta_{J+1}},$$

where

$$\tan\eta_{J,J+1}=-\tan\delta_{J+1}\frac{f_{J,J+1}+\tan\alpha_{J+1}}{f_{J,J+1}+\tan\beta_{J+1}}. \quad (21)$$

As may be readily verified, one of the two solutions of (20) approaches $f_{J,J-1}$, as $f_J^{(t)}$ goes to zero. By suitable redefinitions an equation can similarly be found for which the solution approaches $f_{J,J+1}$, as $f_J^{(t)}$ goes to zero. The mixing parameter $\epsilon_J^{(\alpha)}$ is defined by

$$\tan\epsilon_J^{(\alpha)}=B_J^{(\alpha)}/A_J^{(\alpha)}. \quad (22)$$

If the two possible values of $\epsilon_J^{(\alpha)}$ are $\epsilon_J^{(1)}$ and $\epsilon_J^{(3)}$, then[10] it follows that

$$\tan\epsilon_J^{(1)}\tan\epsilon_J^{(3)}=-1. \quad (23)$$

The equation determining $\epsilon_J^{(\alpha)}$ is

$$\tan\epsilon_J^{(\alpha)}=[(F_J^{(\alpha)}-f_{J,J-1})/f_J^{(t)}](n_{J-1}/n_{J+1})$$
$$\times[(\tan\delta_{J-1}-\tan\eta_J^{(\alpha)})/(\tan\delta_{J+1}-\tan\eta_J^{(\alpha)})]. \quad (24)$$

By expanding the various factors appearing in (19) and (20), it is possible to obtain an energy expansion of $\cot\eta_J^{(\alpha)}$. We give here only the energy expansion for the $J=1$ state, where the principal component at low energy is the $^3S_1$. The expansion of $x_0\cot\eta_1^{(\alpha)}$ is of the form

$$x_0\cot\eta_1^{(\alpha)}\simeq-(r_0/a_1)+\tfrac{1}{2}(\rho_1/r_0)x_0^2-P_1(\rho_0/r_0)^3x_0^4, \quad (25)$$

where a_1 is the scattering length and ρ_1 is the triplet effective range. We find

$$r_0/a_1=1+(1/p),$$
$$\rho_1/2r_0=(1/3)\{1-(1/p)+(1/p^2)[1-(f_1^{(t)})^2/(f_{12}+3)^2]\},$$
$$P_1(\rho_1/r_0)^3=-(1/15)\{(1/3)-(1/p)+(1/p^2)\times[2-(5/3)[(f_1^{(t)})^2/(f_{12}+3)^3]\times[f_{12}+4]]+(1/p^3)[-(5/3)+5(f_1^{(t)})^2/(f_{12}+3)^2-(5/3)\times(f_1^{(t)})^4/(f_{12}+3)^4]\}, \quad (26)$$
$$p=f_{10}-(f_1^{(t)})^2/(f_{12}+3).$$

It will also prove useful to have the low-energy expansions of $F_J^{(\alpha)}$. From Eq. (17) we obtain

$$F_J^{(\alpha)}=f_{J,J-1}-\frac{(f_J^{(t)})^2}{f_{J,J+1}+\tan\beta_{J+1}(1+\tan\delta_{J+1}'\cot\eta_J^{(\alpha)})/(1+\tan\delta_{J+1}\cot\eta_J^{(\alpha)})}.$$

We introduce the quantity $q_J^{(\alpha)}$ by the equation,

$$\cot\eta_J^{(\alpha)}\underset{x_0\to0}{\longrightarrow}-\cot\delta_{J-1}q_J^{(\alpha)}. \quad (27)$$

For $J=1$, $q_1^{(\alpha)}$ equals (r_0/a_1), as can be seen from (25). In terms of these quantities, we obtain

$$F_J^{(\alpha)}\simeq[f_{J,J-1}-(f_J^{(t)})^2/(f_{J,J+1}+J+2)]$$
$$-x_0^2(f_J^{(t)})^2/[(2J+1)(f_{J,J+1}+J+2)^2]$$
$$-x_0^4\frac{(f_J^{(t)})^2}{(2J+1)^2(2J-1)[f_{J,J+1}+J+2]^2}$$
$$\times\left[1-q_J^{(\alpha)}+\frac{2J-1}{f_{J,J+1}+J+2}\right]. \quad (28)$$

We note that to obtain the three quantities $f_{J,J-1}$, $f_{J,J+1}$ and $(f_J^{(t)})$ making up the F_J matrix, the experimental data must be sufficiently well known up to energies at which the x_0^4 term in (28) becomes important. It can be seen that for large values of J, or sufficiently small values of $f_J^{(t)}$, or $f_{J,J+1}\geq0$, the coefficient of x_0^4 can be quite small so that for a good part of the energy range $F_J^{(\alpha)}$ will depend only on low-energy parameters as determined by the first two terms of Eq. (28).

Bound States

Bound singlet systems are described by the wave function

$$\psi_l=A_l h_l^{(1)}(i\beta r)\to A_l e^{-i(l+1)\pi/2}e^{-\beta r}/\beta r \text{ as } r\to\infty. \quad (29)$$

Boundary condition (1) now yields an equation determining β and therefore the binding energy:

$$f_l = i\beta r_0 h_l^{(1)\prime}(i\beta r_0)/h_l^{(1)}(i\beta r_0). \tag{30}$$

A similar equation holds for uncoupled triplet states, such as $l=J$ and $l=1$, $J=0$. One need only replace f_l by the appropriate f_{Jl}. The function on the right-hand side is a monotonic function of βr_0, decreasing as β increases. Its maximum value is $-(l+1)$. Therefore, if f_l is larger than $-(l+1)$, there will be no bound states.

The equation determining the binding energy for a triplet state where coupling through $f_J^{(t)}$ is involved may be obtained from Eq. (18) by substituting $i\beta r_0$ for x_0 and $h^{(1)}(i\beta r_0)$ for $j_l-(\tan\eta)n_l$. Then

$$f_{J,J-1} = i\beta r_0 \frac{h_{J-1}'(i\beta r_0)}{h_{J-1}(i\beta r_0)} + \frac{(f_J^{(t)})^2}{f_{J,J+1} - i\beta r_0 h_{J+1}'(i\beta r_0)/h_{J+1}(i\beta r_0)}. \tag{31}$$

We observe that, if $f_{J,J+1} > -(J+2)$, then a bound state exists only if

$$f_{J,J-1} \leq -J + [(f_J^{(t)})^2/(J+2+f_{J,J+1})]. \tag{32}$$

The mixing parameter $\tan\epsilon_J^{(\alpha)}$ is obtained from

$$\tan\epsilon_J^{(\alpha)} = f_J^{(t)} h_{J-1}(i\beta r_0)/ [i\beta r_0 h_{J+1}'(i\beta r_0) - f_{J,J+1} h_{J+1}(i\beta r_0)]. \tag{33}$$

Cross Sections

The differential and total neutron-proton cross sections for the singlet case are

$$\sigma_{np}^{(0)} = (1/16k^2)\,|\sum_l (2l+1)(e^{2i\eta_l}-1)P_l(\cos\vartheta)\,|^2, \qquad Q_{np}^{(0)} = (\pi/k^2)\sum_l (2l+1)\sin^2\eta_l. \tag{34}$$

We have already included the factor of (1/4) corresponding to the probability of finding the system in a singlet state. In the other formulas of this section below, similar factors will be included. The triplet neutron-proton cross section has been expressed directly in terms of the eigenphases of the S matrix by Blatt and Biedenharn[11]:

$$\sigma_{np}^{(1)} = (1/4k^2)\sum_L B_L P_L(\cos\vartheta),$$
$$B_L = \sum_{J,J',\alpha,\beta} (J^{(\alpha)}\,|\,J'^{(\beta)}) Y(J\alpha J'\beta;1L),$$
$$(J^{(\alpha)}\,|\,J'^{(\beta)}) = \sin\eta_J^{(\alpha)} \sin\eta_{J'}^{(\beta)} \cos(\eta_J^{(\alpha)} - \eta_{J'}^{(\beta)}).$$
$$Y(J\alpha J'\beta;1L) = |\sum_{l,l'} Z(lJl'J';1L)(l'\,|\,a_{J'}^{(\beta)})(a_J^{(\alpha)}\,|\,l)\,|^2. \tag{35}$$

Here Z are coefficients introduced by Biedenharn, Blatt, and Rose[11] and tabulated by Biedenharn.[12] The coefficients $(l\,|\,a_J^{(\alpha)})$ are transformation coefficients from the eigenvectors of the scattering matrix to the l (orbital-angular momentum) representation. The superscript α (or β) takes on three values 1, 2, 3, two of these, 1 and 3, corresponding to the two possible solutions of Eq. (20) for the $l=J\pm1$ states, the third for the $l=J$ state:

$$(a_J^{(\alpha)}\,|\,l) = \begin{bmatrix} \cos\epsilon_J^{(1)} & 0 & \sin\epsilon_J^{(1)} \\ 0 & 1 & 0 \\ -\sin\epsilon_J^{(1)} & 0 & \cos\epsilon_J^{(1)} \end{bmatrix}, \tag{36}$$

where the rows of the matrix are denoted by the value of α and the columns by the possible values of l in ascending numerical value. The total triplet cross section is

$$Q_{np}^{(1)} = (\pi/k^2)\sum_{J,\alpha}(2J+1)\sin^2\eta_J^{(\alpha)}. \tag{37}$$

For proton-proton scattering the wave function must be antisymmetric, with the consequence that all even-l states must be singlets, all odd-l states triplets. Moreover, the amplitudes of each of these must be doubled. Hence, the right-hand side of Eq. (34) must be multiplied by a factor of 4 and all odd-l terms dropped in order to describe singlet proton-proton scattering. For triplet scattering, the right-hand side of Eq. (35) must be multiplied by 4 and all even-l terms omitted in the sum.

Polarization

Experimentally a double scattering is performed, the first angle of scattering being ϑ and the second angle ϑ'. In the second scattering for a given ϑ' the azimuthal variation of the scattered intensity is measured and the following quantity determined

$$\epsilon(\vartheta,\vartheta') = [N(0)-N(\pi)]/[N(0)+N(\pi)],$$

where 0 and π are the value of the azimuthal angle φ. It may be shown that $\epsilon(\vartheta,\vartheta')$ is the product of the polarizations produced on each scattering, i.e.,

$$\epsilon(\vartheta,\vartheta') = p(\vartheta)p(\vartheta').$$

The polarization $p(\vartheta)$ in turn equals the absolute value of the expectation value of the spin in the final state.[13] It has been evaluated in a very general form by Simon and Welton.[14] We shall not give their general result but shall immediately specialize to nucleon-nucleon scattering. To obtain our result from theirs, we require only the matrix elements of the S matrix between two different orbital angular momenta:

$$(l\,|\,1-S\,|\,l') = -2i\sum \sin\eta_J^{(\alpha)} \exp(i\eta_J^{(\alpha)}) \times (l\,|\,a_J^{(\alpha)})(a_J^{(\alpha)}\,|\,l'). \tag{38}$$

We then obtain

$$p_{np} = \sqrt{3}/[2k^2\sigma_{np}(\vartheta)]\sum P_L^{(1)}(-)^J(2J+1)(2J^*+1) \times [J^{(\alpha)}\,|\,J^{*(\beta)}]M(J,\alpha,J^*,\beta;L)N(J,\alpha,J^*,\beta;L), \tag{39}$$

[11] Biedenharn, Blatt, and Rose, Revs. Modern Phys. **24**, 249 (1952).
[12] L. C. Biedenharn, Oak Ridge National Laboratory Report ORNL-1501, May, 1953 (unpublished).
[13] L. Wolfenstein, Phys. Rev. **75**, 1664 (1949).
[14] A. Simon and T. Welton, Phys. Rev. **90**, 1036 (1953).

where

$$[J^{(\alpha)}|J^{*(\beta)}]=\sin\eta_J{}^{(\alpha)}\sin\eta_{J^*}{}^{(\beta)}\sin(\eta_J{}^{(\alpha)}-\eta_{J^*}{}^{(\beta)}),$$

$$M(J,\alpha,J^*,\beta;L)=\sum i^{l_2-l_1}[(2l_1+1)(2l_2+1)]^{\frac{1}{2}}(l_1l_200|l_1l_2L0)\times W(l_1Jl_2J^*;1L)(l_2|a_{J^*}{}^{(\beta)})(a_J{}^{(\alpha)}|l_1), \quad (40)$$

and

$$N(J,\alpha,J^*\beta;L)=\sum i^{-(l_1'+l_2')}[(2l_1'+1)(2l_2'+1)]^{\frac{1}{2}}(l_1'l_2'00|l_1'l_2'L0)\times X(Jl_1'1;J^*l_2'1;LL1)(a_{J^*}{}^{(\beta)}|l_2')(l_1'|a_J{}^{(\alpha)}). \quad (41)$$

Here J and J^* are possible J values of the system, l_i possible incident orbital angular momenta, l_i' possible orbital angular momenta of the emergent beam. The factors $(l_1l_200|l_1l_2L0)$ are Clebsch-Gordan coefficients, W is the Racah coefficient[15] and X is the Wigner $9j$ symbol,[16] where we have employed the definition of Fano and Racah, as given in Appendix B of Simon and Welton's paper.[14] In Eq. (39) the sums are take over all possible values of L, α, β, J, $(J+L)\geq J^*\geq|(J-L)|$. In Eqs. (40) and (41) the sums are taken over all values of l_1 and l_2 consistent with the values of J, J^*, and L. The cross section $\sigma_{np}(\vartheta)$is the singlet plus the triplet cross section. Finally, $P_L{}^{(1)}$ is the normalized associated Legendre function. For $p-p$ scattering, Eq. (39) applies if on the right-hand side a factor of 4 is inserted in the numerator, σ_{np} is replaced by σ_{pp} in the denominator and finally if in M and N only odd l_i and l_i' are included in their defining sums.

III. LOW-ENERGY DATA

Proton-Proton Scattering

The low-energy data have been analyzed and fitted to a boundary condition by Breit and Bouricius.[5] The parameters $f^{(n)}$ in Eq. (14) are related to their $\nu^{(n)}$ by

$$\nu^{(n)}=(40.0)^n f^{(n)}.$$

Using the experimental values of $\nu^{(0)}=7.805\pm0.02$, $\nu^{(1)}=0.925\pm0.03$, Eq. (15) may be solved for r_0 and the boundary parameter f_0. We expect f_0 to be somewhat greater than (-1) since this value corresponds to zero binding for two protons. We find

$$f_0=0.082-1, \qquad r_0=1.32\times10^{-13}\text{ cm}. \quad (42)$$

These parameters give $\nu^{(0)}=7.79$ and $\nu^{(1)}=0.928$ and predicts $\nu^{(2)}=0.0074$, which is to be compared with the experimental value $\nu^{(2)}=\pm0.01$. Our results are substantially the same as those of Breit and Bouricius. The cut-off distance r_0 is nearly equal to the meson Compton wavelength and is therefore of the expected order of magnitude.

Singlet Neutron-Proton Scattering

The data here are[17]

$$a_0=(-23.7\pm0.1)\times10^{-13}\text{ cm},$$
$$\rho_0=(2.7\pm0.5)\times10^{-13}\text{ cm},$$
$$P_0=-0.04.$$

Since the value of ρ_0 is not very well known, we shall content ourselves with assuming the same cut-off radius as in Eq. (42) determining f_0, predicting ρ_0 and P_0. We find $f_0=0.053-1$, $\rho_0=2.79\times10^{-13}$ cm, $P_0=-0.039$. These are in accord, so that it is consistent with the data to use the same core radius for both $p-p$ and $n-p$ ^1S interactions. The small difference between the f_0 for singlet $n-p$ scattering and that for $p-p$ scattering reveals a deviation from charge independence, which, of course, is well known from potential model studies. We shall assume, as Schwinger[18] has demonstrated for some potentials, that this deviation arises from the differences in the magnetic interaction between the two systems. We shall make no attempt to compute this effect here since it is quite sensitive to the behavior of the wave functions at small values of r and therefore in the present model on the electromagnetic properties of the core. Fortunately the difference in f_0 is of no consequence for the analysis of high-energy data, for which we shall use $f_0=0.053-1$.

Triplet Neutron-Proton Scattering

The fundamental data[17] are the scattering length $(5.39\pm0.03)\times10^{-13}$ cm, and the effective range $\rho_1=(1.703\pm0.03)\times10^{-13}$ cm. From Eq. (26) the combinations p and $(f_1{}^{(t)}/f_{12}+3)^2$ can be determined for $r_0=1.32\times10^{-13}$ cm. We obtain

$$p=-1.325, \quad [f_1{}^{(t)}/(f_{12}+3)]^2=0.640.$$

These two relations do not suffice to determine the three parameters describing F_1. Some idea as to the effect of three different choices of f_{12} can be seen from Table I, where W is the coefficient of the x^4 term in Eq. (28) for the effective F. Note that this is the only term in (28) sensitive to the value of f_{12}. We see that, except for f_{12} nearly equal to -3, which is not admissible since it gives rise to a low-lying D resonance, F is quite insensitive to the precise value of f_{12} up to comparatively high-energy values. For example, at $x^2=2$, corresponding to nearly 100 Mev, the x^4 term

[15] G. Racah, Phys. Rev. **62**, 442 (1942); Biedenharn, Blatt, and Rose, Revs. Modern Phys. **24**, 249 (1952). The Racah coefficients have been tabulated by L. C. Biedenharn in an Oak Ridge National Laboratory Report ORNL-1098 (unpublished).

[16] E. P. Wigner, "On the Matrices which Reduce the Kronecker Products of Representations of Simply Reducible Groups," (unpublished); J. Schwinger, U. S. Atomic Energy Commission Report NYO-3071, Nuclear Development Associates, Inc., White Plains, New York, 1952 (unpublished); H. A. Jahn and J. Hope, Phys. Rev. **93**, 318 (1954); U. Fano and G. Racah (unpublished); U. Fano, National Bureau of Standards Report 1214 (unpublished), p. 48. The X function is tabulated for a limited range of parameters by Sharp, Kennedy, Sears, and Hoyle, Atomic Energy of Canada, Limited, Report No. 97 (unpublished).

[17] E. E. Salpeter, Phys. Rev. **82**, 60 (1951).

[18] J. Schwinger, Phys. Rev. **78**, 135 (1950).

contributes only about 10% to F. This leads to the important result, for which we shall later present further evidence, that $^3S_1+^3D_1$ contribution to the triplet neutron-proton scattering up to about 100 Mev can be deduced from the low-energy data.

The Deuteron

The binding energy of the deuteron must be given correctly by the above choices since it is not essentially independent of the low-energy triplet scattering data. We cannot give a precise value for the deuteron's electromagnetic properties since we do not know the electromagnetic properties of the core region $r<r_0$. However, it is important that the contribution made by the region outside the core be of the proper order of magnitude so that the core itself not be required to make an unreasonably large contribution. We shall be concerned with the quadrupole moment Q and the fraction of D state, p_D. Denoting by a prime the values obtained for these quantities dropping contributions both to it and the normalization integrals inside the core, we obtain

$$\begin{aligned} p_D' &= 2\lambda \tan^2\epsilon_1^{(1)}/[1+\lambda \tan^2\epsilon_1^{(1)}], \\ \lambda &= \tfrac{1}{2}+3(R_0/r_0)+6(R_0/r_0)^2+3(R_0/r_0)^3, \\ Q' &= (2\tfrac{2}{3}/10)R_0^2 \tan\epsilon_1^{(1)}\{\tfrac{1}{2}[5+4(r_0/R_0) \\ &\quad +(r_0/R_0)^2]-(\tan\epsilon_1^{(1)}/8\tfrac{1}{3})[9(R_0/r_0)+9 \\ &\quad +(27/4)((r_0/R_0)+(r_0/R_0)^2)] \\ &\quad \times[\tfrac{1}{2}+\lambda \tan^2\epsilon_1^{(1)}]\}^{-1}, \\ \tan\epsilon_1^{(1)} &= -f_1^{(t)}\{1+(r_0/R_0)+(3+f_{12}) \\ &\quad \times[1+3(R_0/r_0)+3(R_0/r_0)^2]\}^{-1}. \end{aligned} \tag{43}$$

Here R_0 is the deuteron "radius," 4.32×10^{-13} cm. We note that, in order that Q have the right sign, $\tan\epsilon_1^{(1)}$ must be positive. In the expression for $\tan\epsilon_1^{(1)}$, the coefficient of the $(3+f_{12})$ term is large compared with $(1+r_0/R_0)$ so that except for f_{12} close to (-3) we may drop $(1+r_0/R_0)$. Then $\tan\epsilon_1^{(1)}$ and therefore Q' and p_D' are determined by the low-energy scattering data, and we may compute the resultant p_D' and Q' for the region outside of r_0. We find $p_D'=0.11$ and $Q'=2.5\times10^{-27}$ cm^2, which are to be compared with the experimental values $p_D=0.04\pm0.02$ and $Q=(2.738\pm0.016)\times10^{-27}$ cm^2. Since p_D is more sensitive than Q to the contributions for $r<r_0$, these results are entirely reasonable.

IV. HIGH-ENERGY DATA

The qualitative properties of the high-energy data to which we shall pay particular attention are as follows: For $p-p$ scattering the main features include, first, the near isotropy of the nuclear scattering for nearly all energies. This isotropy is not perfect as has been demonstrated by experiments at Harvard[19] and California.[20] Secondly the cross section at 90° is relatively independent of the proton energy for energies exceeding 100 Mev. A third feature is the measurement of $p-p$ polarization which, considering only energies less than 275 Mev, the maximum energy treated in this paper, has been measured at 135 Mev[21] and 240 Mev.[22] The polarization has been found to be approximately the same at these two energies, and the indications are that the sign is positive.[23] The present data indicate an angular distribution more complex than $\sin2\vartheta$ and therefore indicates that states with l higher than one are involved. In our discussion we shall neglect Coulomb effects which in principle would help determine phase shift signs and which for the lower energies would affect the determination of the anisotropy of the $p-p$ scattering. We hope to consider these effects in more detail in a later paper. Another omission will be the angular distribution of the polarization experiments. Only the magnitude of 20° (laboratory angle) employing just the $\sin2\vartheta$ term will be matched.

TABLE I. Effect of f_{12} upon low-energy scattering.

f_{12}	f_{10}	$f_1^{(t)}$	ρ_1	P	W
1.725	1.725	−3.80	1.72×10^{-13} cm	−0.034	0.068
−1.38	−0.696	−1.285	1.72×10^{-13}	−0.027	0.098
−2.80	−1.187	−0.160	1.72×10^{-13}	0.054	0.410

The principal features of the $n-p$ data which are of interest include the total cross section and the angular distribution. The former, after decreasing from about 200 mb at 40 Mev to about 50 mb at 130 Mev, remains relatively constant up to 270 Mev. The angular distribution is anisotropic but symmetric about 90° up to 100 Mev. By 300 Mev the angular distribution is definitely peaked in the backward direction. This asymmetry sets in possibly as early as 135 Mev.[24]

Charge independence, which we shall of course assume, implies certain relationships between $n-p$ and $p-p$ scattering. The scattering amplitude for $p-p$ scattering can be written in operator form as follows:

$$\mathbf{f}_{pp}{}^{(\vartheta)}=2[f_{se}\mathbf{P}_s+f_{to}\mathbf{P}_t],$$

where $\mathbf{P}_s$ and $\mathbf{P}_t$ are the well-known projection operators for the singlet and triplet states, f_{se} and f_{to} are the corresponding scattering amplitudes which are even and odd respectively against an inversion. The scattering amplitude for $(n-p)$ scattering in the same notation is

$$\mathbf{f}_{np}{}^{(\vartheta)}=(f_{se}+f_{so})\mathbf{P}_s+(f_{te}+f_{to})\mathbf{P}_t.$$

The scattering at $(\pi-\vartheta)$, is then

$$\mathbf{f}_{np}(\pi-\vartheta)=(f_{se}-f_{so})\mathbf{P}_s-(f_{te}-f_{to})\mathbf{P}_t,$$

[19] Kruse, Teem, and Ramsey, Phys. Rev. **94**, 1795 (1954).
[20] D. Fischer and G. Goldhaber, Phys. Rev. **95**, 1350 (1954).
[21] J. M. Dickson and D. C. Salter, Nature **173**, 946 (1954).
[22] Oxley, Cartwright, and Rouvina, Phys. Rev. **93**, 806 (1954).
[23] Proceedings of the Fifth Annual Rochester Conference (Interscience Publishers, New York, 1955), p. 146.
[24] Randle, Taylor, Wood, and Snowden, Report on the Birmingham Conference on Nuclear Physics, June, 1953 (unpublished), p. 25. Combining the data of Thresher, Voss, and Wilson, Proc. Roy. Soc. (London) **A229**, 492 (1955), and T. C. Randle and E. Uridge (unpublished), we estimate $\sigma(180°)/\sigma(0)\sim1.3$ at 135 Mev.

where we have inserted a phase of (-1) for the singlet as opposed to the triplet scattering which we can do since these do not interfere. Combining the last three equations we have the vector relation[25]

$$\mathbf{f}_{np}(\vartheta)+\mathbf{f}_{np}(\pi-\vartheta)=\mathbf{f}_{pp}(\vartheta), \tag{44}$$

which expresses in a succinct form the consequences of charge independence.

Some of the consequences are of interest. First we have the general vector inequalities:

$$|\sigma_{np}^{\frac{1}{2}}(\pi-\vartheta)-\sigma_{np}^{\frac{1}{2}}(\vartheta)| \leq \sigma_{pp}(\vartheta) \leq \sigma_{np}^{\frac{1}{2}}(\pi-\vartheta)+\sigma_{np}^{\frac{1}{2}}(\vartheta).$$

For $\vartheta=90°$ and $\vartheta=180°$, we have respectively

$$\sigma_{pp}(\pi/2) \leq 4\sigma_{np}(\pi/2), \quad \sigma_{np}^{\frac{1}{2}}(\pi)-\sigma_{np}^{\frac{1}{2}}(0) \leq \sigma_{pp}^{\frac{1}{2}}(0).$$

The first of these inequalities is always satisfied by the experimental data. In the second, over most of the energy range an estimate of the specifically nuclear $p-p$ cross section $\sigma_{pp}(0)$ may be obtained by assuming isotropy. The second inequality is just barely met by the $n-p$ data of de Pangher at 300 Mev, but is easily satisfied by Easely's data, which give a larger $\sigma_{np}(0)$ at the same energy. At higher energies the proton-proton scattering becomes peaked in the forward direction, as it must in order to match the large back-to-forward ratio of the measured $n-p$ scattering.[26]

Proton-Proton Scattering

We shall first give the necessary detailed formulas as obtained from Eqs. (34) and (35). The differential cross section including both the singlet and triplet contributions is

$$\sigma_{pp}(\vartheta)=(1/k^2)\sum_L B_L^{(1)} P_L(\cos\vartheta), \tag{45}$$

where the superscript on B indicates that the isotopic spin under consideration is 1. For $p-p$ scattering only even L enter. Let

$$(Jl|J'l')=\sin\eta_{Jl}\sin\eta_{J'l'}\cos(\eta_{Jl}-\eta_{J'l'}) \tag{46}$$

for triplet states. When coupling between states of different l's is possible, we shall use the symbol

$$(J^{(\alpha)}|J'^{(\beta)})=\sin\eta_J^{(\alpha)}\sin\eta_{J'}^{(\beta)}\cos(\eta_J^{(\alpha)}-\eta_{J'}^{(\beta)}), \tag{47}$$

where $\eta_J^{(\alpha)}$ is an eigenphase as defined by Eq. (17). For singlet states since $l=J$ we drop l and l' in the symbol defined by Eq. (46). We then find

$$B_0^{(1)}=(0|0)+(01|01)+3(11|11)+5(2|2)+5(2^{(1)}|2^{(1)})+5(2^{(3)}|2^{(3)})+7(33|33)+9(4|4), \tag{48a}$$

$$\begin{aligned}B_2^{(1)}=&(3/2)(11|11)+10(0|2)+(50/7)(2|2)+12(11|33)+(21/4)(33|33)\\&+4[\cos\epsilon_2^{(1)}+(3/2)^{\frac{1}{2}}\sin\epsilon_2^{(1)}]^2(2^{(1)}|01)+4[-\sin\epsilon_2^{(1)}+(3/2)^{\frac{1}{2}}\cos\epsilon_2^{(1)}]^2(2^{(3)}|01)\\&+3[\cos\epsilon_2^{(1)}-(2/3)^{\frac{1}{2}}\sin\epsilon_2^{(1)}]^2[3(11|2^{(1)})+2(33|2^{(1)})]\\&+3[\sin\epsilon_2^{(1)}+(2/3)^{\frac{1}{2}}\cos\epsilon_2^{(1)}]^2[3(11|2^{(3)})+2(33|2^{(3)})]\\&+(7/2)[\cos^2\epsilon_2^{(1)}+(24/49)^{\frac{1}{2}}\sin\epsilon_2^{(1)}\cos\epsilon_2^{(1)}+(8/7)\sin^2\epsilon_2^{(1)}]^2(2^{(1)}|2^{(1)})\\&+7[(1/7)\cos\epsilon_2^{(1)}\sin\epsilon_2^{(1)}+(6/49)^{\frac{1}{2}}\cos2\epsilon_2^{(1)}]^2(2^{(1)}|2^{(3)})\\&+(7/2)[\sin^2\epsilon_2^{(1)}-(24/49)^{\frac{1}{2}}\sin\epsilon_2^{(1)}\cos\epsilon_2^{(1)}+8/7\cos^2\epsilon_2^{(1)}]^2(2^{(3)}|2^{(3)}),\end{aligned} \tag{48b}$$

$$\begin{aligned}B_4^{(1)}=&(90/7)(2|2)+9(33|11)+(7/22)(33|33)+60/7[\sin2\epsilon_2^{(1)}-(1/6)^{\frac{1}{2}}\sin^2\epsilon_2^{(1)}]^2(2^{(1)}|2^{(1)})\\&+(120/7)[\cos2\epsilon_2^{(1)}+(1/6)^{\frac{1}{2}}\sin\epsilon_2^{(1)}\cos\epsilon_2^{(1)}]^2(2^{(1)}|2^{(3)})\\&+(60/7)[-\sin2\epsilon_2^{(1)}+(1/6)^{\frac{1}{2}}\cos^2\epsilon_2^{(1)}]^2(2^{(3)}|2^{(3)})\\&+50[\sin\epsilon_2^{(1)}-(3/10)^{\frac{1}{2}}\cos\epsilon_2^{(1)}]^2(33|2^{(1)})\\&+50[\cos\epsilon_2^{(1)}+(3|10)^{\frac{1}{2}}\sin\epsilon_2^{(1)}]^2(33|2^{(3)}).\end{aligned} \tag{48c}$$

These formulas include contributions from $^1S_0$, $^1D_2$, $^3P_0$, $^3P_1$, $^3P_2+^3F_2$, and $^3F_3$ states. The parameter $\epsilon_2^{(1)}$ measures the mixing of $^3P_2$ and $^3F_2$ states by way of the matrix F_2; $\epsilon_2^{(1)}=0$ corresponds to no coupling between these states.

We turn now to the data and consider first the isotropy. The simplest solution of this problem is to make the principal states involved be the $^1S_0$ and the $^3P_0$, since both of these give rise to isotropic distributions. It is, of course, possible at any given energy to obtain isotropy by a suitable mixture of many states, but it would be very difficult in any theory to maintain the necessary delicate balance over the required large energy range. To determine qualitatively what the appropriate value for the boundary parameter f_{01} should be, we first determine roughly the contribution of the $^1S_0$ state by assuming r_0 (we shall for convenience never vary the boundary parameters with energy) to be energy-independent. We find that the phase shift decreases with increasing energy, going through zero at about 120 Mev and then changing sign and becoming of some importance at 300 Mev. This behavior is very similar to that obtained by Jastrow in his hard-core model. To obtain the results given by the monotonic potentials, it would be necessary to have r_0 decrease very rapidly and eventually become negative, indicating for that case the absence of any physical significance to the core radius. However, in either event it is necessary for the $^3P_0$ state to make a very sizeable contribu-

[25] J. Schwinger (unpublished).

[26] Hartzler, Siegel, and Opitz, Phys. Rev. **95**, 591 (1954); A. J. Hartzler and R. T. Siegel, Phys. Rev. **95**, 185 (1954).

tion to the cross section. A second consideration limiting the possible choices of f_{01} comes from $n-p$ scattering, in which the interference terms between the $^3P_0$ state and the $(^3S_1+^3D_1)$ states are critical for the angular distribution. We find that to have symmetry about 90° below 100 Mev and a backward peak at higher energies, it is essential that the $^3P_0$ phase shift be negative. Of course, evidence bearing on this sign would also become available upon analyzing the effects of Coulomb interference.[27] The dependence of the phase shifts on f_{01} is shown in Fig. 1. Combined with the results for the $^1S_0$ state we find that, to obtain the observed $\sigma_{pp}(90°)$, f_{01} should be between -5 and $-\infty$, the particular value depending upon the energy dependence assumed for the core radius for the $^1S_0$ state.

To go further in this analysis we must consider the polarization data. We define the symbol $[Jl|J'l']'$ and the analog of (47) by

$$[Jl|J'l']=\sin\eta_{Jl}\sin\eta_{J'l'}\sin(\eta_{Jl}-\eta_{J'l'}).$$

Then from (39) the $\sin 2\vartheta$ term is

$$p_{pp}=3(\sin 2\vartheta/k^2\sigma_{pp})[(\cos 2\epsilon_2^{(1)}+(1/6)^{\frac{1}{2}}\sin 2\epsilon_2^{(1)}) \times([01|2^{(1)}]-[01|2^{(3)}]+\tfrac{3}{2}[11|2^{(1)}]-\tfrac{3}{2}[11|2^{(3)}]) +(5/4)[2/7+(1/6)^{\frac{1}{2}}]\cos 2\epsilon_2^{(1)}[2^{(1)}|2^{(3)}]]+\cdots. \quad (49)$$

TABLE II. Angular distribution coefficients $B_L^{(1)}$. Entries not made are negligible.

Energy (Mev)		38.5	80	120	190	274
$B_0^{(1)}$	A	0.505	0.474	0.564	0.875	1.232
	B	0.490	0.430	0.579	0.825	1.102
$B_2^{(1)}$	A	−0.007	−0.001	−0.036	0.012	0.095
	B	−0.014	−0.004	−0.020	0.032	0.030
$B_3^{(1)}$	A					
	B		0.011	−0.011	−0.015	−0.057

We first look only at the terms involving the $^3P_0$ state, taking $\epsilon_2^{(1)}=0$. (We have considered the effect of including coupling between the $^3P_2$ and the $^3F_2$ but have found that there is no particular advantage gained for the matching of the presently available experimental data, so that in the discussion below $\epsilon_2^{(1)}=0$.) Two possible alternatives suggest themselves. In alternative A we assume that the $^3F_2$ phase shift is small at all energies and that burden of matching the polarization must be carried by the $^3P_2$ phase shift alone. In alternative B the $^3P_2$ phase shift is mainly responsible for the polarization at low energies, while the $^3F_2$ takes over at high energies. Having thus specified the $^3P_2$ and $^3F_2$ phase shifts at two energies, the core radius and boundary condition parameter for each are determined; again these parameters are assumed to be energy independent. From these quantities the phase shifts for other energies could be found.

Starting from this basis, various values of f_{01} were tried. The limiting features were (1) the nature of the interference with the $^3P_2$ and $^3F_2$ states; (2) the required $p-p$ cross section at 90°; (3) the effect on $n-p$ angular distributions. By keeping f_{01} close to infinity, effects (1) and (3) were made optimal. However, if f_{01} were infinity, requirement (2) would not be easily met. A compromise was made by taking $f_{01}=-16$, a choice which did not yield a large enough cross section at 90° for the lower energies. The anisotropy which arose from the interference between this $^3P_0$ state and the $^3P_2$ and $^3F_2$ states could not be cancelled out to a sufficient degree by the interference of the latter states with the $^3P_1$ and at the same time maintain a correct $n-p$ angular distribution. It was then necessary that the major term which would restore isotropy should arise from the interference of the $^1S_0$ and $^1D_2$ states. Again assuming energy-independent boundary conditions for the $^1D_2$ state, it was found necessary for alternative A that the $^1S_0$ phase shift not go through a zero, and for alternative B that the $^1S_0$ phase shift have its zero at a somewhat greater energy than would be obtained if the low-energy parameters were kept constant. To accomplish this the core radius for the $^1S_0$ state is permitted to have a relatively slow energy dependence. Once $B_0^{(1)}$ and $B_2^{(1)}$ have been properly adjusted, it is necessary to examine the value of the $B_4^{(1)}$ coefficient. For alternative A this coefficient was negligible, while for alternative B some additional $^3F_3$ was required,

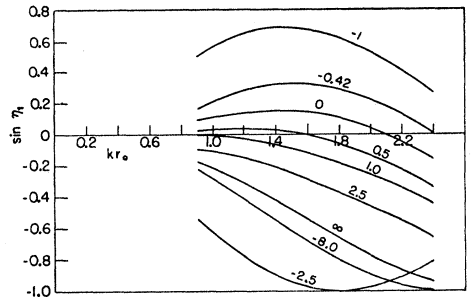

FIG. 1. Phase shifts for uncoupled P states as a function of wave number and boundary parameter. The latter is indicated on each curve.

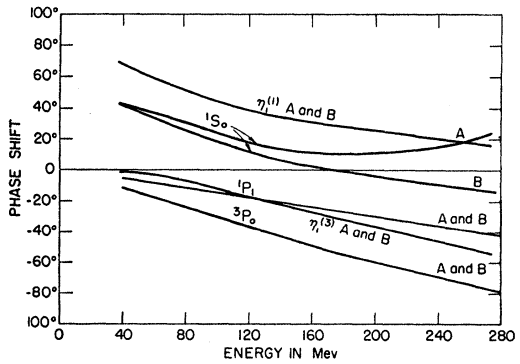

FIG. 2. Phase shifts as a function of energy for cases A and B.

[27] R. M. Thaler and J. Bengston, Phys. Rev. **94**, 679 (1954); A. Garren, Phys. Rev. **96**, 1709 (1954).

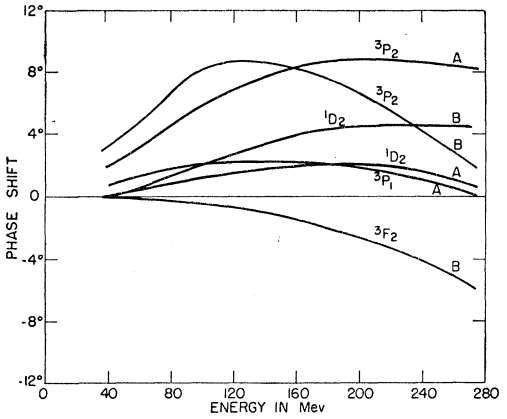

FIG. 3. Phase shifts as a function of energy for cases A and B.

which in turn modified $B_2^{(1)}$. The final values of the parameters are given in Table IV, to be found in Sec. V, the Conclusions, and the resultant values of the coefficients $B_2^{(1)}$ in Table II. The only substantial deviation from complete isotropy occurs at 274 Mev, where for alternative A $B_2^{(1)}/B_0^{(1)}$ is 0.077, which is not in disagreement with the experiments. The phase shifts are exhibited in Fig. 2 and Fig. 3. The resultant cross section at 90° is given in Fig. 4 and is satisfactorily within experimental error of the data for the most of the range, although it is somewhat low for energies between 40 and 80 Mev. The polarization is given in Fig. 5 in terms of the coefficient of the $\sin 2\vartheta$ term in Eq. (49).

It should be noted that the choice of parameters is fairly unique once the $^3P_2$ and $^3F_2$ phase shifts are set. Of course, this is true only if one insists on keeping the boundary conditions as energy independent as possible. One result seems, however, to be relatively mode-independent, and that is that the scattering in the $^3P_0$ state is close to that of an infinitely repulsive sphere.

Neutron-Proton Scattering

The differential cross section including both singlet and triplet contributions is

$$\sigma_{np}(\vartheta)=(1/4k^2)\sum_L B_L P_L(\cos\vartheta), \tag{50}$$

where

$$B_L=B_L^{(1)}+B_L^{(0)}. \tag{51}$$

Expressions for $B_L^{(1)}$ are given in Eq. (48). The corresponding expressions for $B_L^{(0)}$ follow

$$B_0^{(0)}=3(1^{(1)}|1^{(1)})+3(1^{(3)}|1^{(3)})+3(1|1)+5(22|22)+7(3|3)+7(32|32), \tag{52a}$$

$$\begin{aligned}B_1^{(1)}=B_1=&6(0|1)+12(1|2)+9(11|22)+18(2|3)+16(33|22)\\&+(-\sin\epsilon_1^{(1)}+2^{\frac{1}{2}}\cos\epsilon_1^{(1)})^2[2(1^{(3)}|01)+3(1^{(1)}|11)]\\&+(\cos\epsilon_1^{(1)}+2^{\frac{1}{2}}\sin\epsilon_1^{(1)})^2[2(1^{(1)}|01)+3(1^{(3)}|11)]\\&+10(\cos\epsilon_1^{(1)}\cos\epsilon_2^{(1)}+50^{-\frac{1}{2}}\sin\epsilon_1^{(1)}\cos\epsilon_2^{(1)}+(27/25)^{\frac{1}{2}}\sin\epsilon_1^{(1)}\sin\epsilon_2^{(1)})^2(1^{(1)}|2^{(1)})\\&+10(-\sin\epsilon_1^{(1)}\cos\epsilon_2^{(1)}+50^{-\frac{1}{2}}\cos\epsilon_1^{(1)}\cos\epsilon_2^{(1)}+(27/25)^{\frac{1}{2}}\cos\epsilon_1^{(1)}\sin\epsilon_2^{(1)})^2(1^{(3)}|2^{(1)})\\&+10(\cos\epsilon_1^{(1)}\sin\epsilon_2^{(1)}+50^{-\frac{1}{2}}\sin\epsilon_1^{(1)}\sin\epsilon_2^{(1)}-(27/25)^{\frac{1}{2}}\sin\epsilon_1^{(1)}\cos\epsilon_2^{(1)})^2(1^{(1)}|2^{(3)})\\&+10(\sin\epsilon_1^{(1)}\sin\epsilon_2^{(1)}-50^{-\frac{1}{2}}\cos\epsilon_1^{(1)}\sin\epsilon_2^{(1)}+(27/25)^{\frac{1}{2}}\cos\epsilon_1^{(1)}\cos\epsilon_2^{(1)})^2(1^{(3)}|2^{(3)})\\&+3(\cos\epsilon_2^{(1)}-(2/3)^{\frac{1}{2}}\sin\epsilon_2^{(1)})^2(2^{(1)}|22)+3(\sin\epsilon_2^{(1)}+(2/3)^{\frac{1}{2}}\cos\epsilon_2^{(1)})^2(2^{(3)}|22)\\&+(84/5)(\cos\epsilon_2^{(1)}+(294)^{-\frac{1}{2}}\sin\epsilon_2^{(1)})^2(2^{(1)}|32)+(84/5)(\sin\epsilon_2^{(1)}-(294)^{-\frac{1}{2}}\cos\epsilon_2^{(1)})^2(2^{(3)}|32),\end{aligned} \tag{52b}$$

$$\begin{aligned}B_2^{(0)}=&6(1|1)+(25/14)(22|22)+(40/7)(32|22)+(48/7)(32|32)\\&+3(\sin 2\epsilon_1^{(1)}+2^{-\frac{1}{2}}\sin^2\epsilon_1^{(1)})^2(1^{(1)}|1^{(1)})+3(-\sin 2\epsilon_1^{(1)}+2^{-\frac{1}{2}}\cos^2\epsilon_1^{(1)})^2(1^{(3)}|1^{(3)})\\&+6(\cos 2\epsilon_1^{(1)}-2^{-\frac{1}{2}}\sin\epsilon_1^{(1)}\cos\epsilon_1^{(1)})^2(1^{(3)}|1^{(1)})+10(\sin\epsilon_1^{(1)}+2^{-\frac{1}{2}}\cos\epsilon_1^{(1)})^2(22|1^{(3)})\\&+10(\cos\epsilon_1^{(1)}-2^{-\frac{1}{2}}\sin\epsilon_1^{(1)})^2(22|1^{(1)})+14(\cos\epsilon_1^{(1)}+(2/49)^{\frac{1}{2}}\sin\epsilon_1^{(1)})^2(32|1^{(1)})\\&+14(\sin\epsilon_1^{(1)}-(2/49)\cos\epsilon_1^{(1)})^2(32|1^{(3)}),\end{aligned} \tag{52c}$$

$$\begin{aligned}B_3^{(0)}=B_3=&6(01|32)+12(11|32)+14(0|3)+18(1|2)+(56/3)(2|3)+(7/3)(33|22)+(28/3)(33|32)\\&+10(\cos\epsilon_1^{(1)}\sin\epsilon_2^{(1)}+(27/25)^{\frac{1}{2}}\sin\epsilon_1^{(1)}\cos\epsilon_2^{(1)}+(8/25)^{\frac{1}{2}}\sin\epsilon_1^{(1)}\sin\epsilon_2^{(1)})^2(1^{(1)}|2^{(1)})\\&+10(-\sin\epsilon_1^{(1)}\sin\epsilon_2^{(1)}+(27/25)^{\frac{1}{2}}\cos\epsilon_1^{(1)}\cos\epsilon_2^{(1)}+(8/25)^{\frac{1}{2}}\cos\epsilon_1^{(1)}\sin\epsilon_2^{(1)})^2(1^{(3)}|2^{(1)})\\&+10(\cos\epsilon_1^{(1)}\cos\epsilon_2^{(1)}-(27/25)^{\frac{1}{2}}\sin\epsilon_1^{(1)}\sin\epsilon_2^{(1)}+(8/25)^{\frac{1}{2}}\sin\epsilon_1^{(1)}\cos\epsilon_2^{(1)})^2(1^{(1)}|2^{(3)})\\&+10(\sin\epsilon_1^{(1)}\cos\epsilon_2^{(1)}+(27/25)^{\frac{1}{2}}\cos\epsilon_1^{(1)}\sin\epsilon_2^{(1)}-(8/25)^{\frac{1}{2}}\cos\epsilon_1^{(1)}\cos\epsilon_2^{(1)})^2(1^{(3)}|2^{(3)})\\&+14(\cos\epsilon_1^{(1)}-2^{-\frac{1}{2}}\sin\epsilon_1^{(1)})^2(1^{(1)}|33)+14(\sin\epsilon_1^{(1)}+2^{-\frac{1}{2}}\cos\epsilon_1^{(1)})^2(1^{(3)}|33)\\&+12(\cos\epsilon_2^{(1)}-(2/3)^{\frac{1}{2}}\sin\epsilon_2^{(1)})^2(2^{(1)}|22)+12(\sin\epsilon_2^{(1)}+(2/3)^{\frac{1}{2}}\cos\epsilon_2^{(1)})^2(2^{(3)}|22)\\&+(36/5)(\cos\epsilon_2^{(1)}+(8/27)^{\frac{1}{2}}\sin\epsilon_2^{(1)})^2(2^{(1)}|32)+(36/5)(-\sin\epsilon_2^{(1)}+(8/27)^{\frac{1}{2}}\cos\epsilon_2^{(1)})^2(2^{(3)}|32),\end{aligned} \tag{52d}$$

$$\begin{aligned}B_4^{(0)}=&24(1|3)+(378/37)(3|3)+(40/7)(22|22)+(100/7)(32|22)+(22/7)(32|32)\\&+(108/7)\sin^2\epsilon_1^{(1)}(1^{(1)}|32)+(108/7)\cos^2\epsilon_1^{(1)}(1^{(3)}|32).\end{aligned} \tag{52e}$$

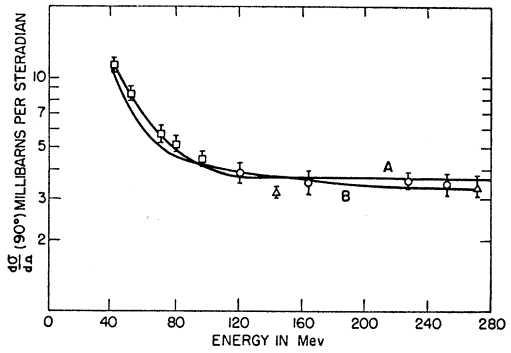

FIG. 4. Differential $p-p$ cross section at 90° in the center-of-mass system as a function of proton laboratory energy. Square points are from Kruse, Teem, and Ramsey [Phys. Rev. 94, 1795 (1954)]. Circular points are from Chamberlain, Segrè, and Wiegand [Phys. Rev. 83, 923 (1951)]. The triangular points are from Marshall, Marshall, and Nedzel [Phys. Rev. 92, 834 (1953)].

The isotopic singlet states which have been considered are ${}^3S_1+{}^3D_1$, ${}^1P_1$, ${}^3D_2$, ${}^3D_3$, ${}^1F_3$.

In our analysis of the $n-p$ data we shall first examine the consequences of the low-energy fit for the ${}^3S_1+{}^3D_1$ state, in which only two combinations of the three parameters of the F_1 matrix have been determined. The parameter f_{12} will be taken to be the remaining unknown to be fixed presumably by the high-energy data. In Fig. 6 we plot the coefficient B_0 (which is directly proportional to Q_{np}) as a function of f_{12} for three energies 38.5, 93 and 260 Mev. The experimental values are also indicated. The contributions included in B_0 are those of the ${}^3S_1+{}^3D_1$ states and of the isotopic triplet state as determined by the experimental proton-proton values. Therefore this B_0 is less than or equal to the actual experimental value, and particularly for the highest energy should be considerably less than the experimental value. From the figure we see that the parameter f_{12} should be greater than zero. But in this range the ${}^3S_1+{}^3D_1$ contributions below about 100 Mev are independent of f_{12} and therefore are completely determined by the low-energy scattering. We note that over most of the energy range nearly all of Q_{np} is given by the ${}^3S_1+{}^3D_1$ states plus the isotopic triplet states.

For the lower energies, the value of B_2 can be calculated from the differential cross section at 90° and is

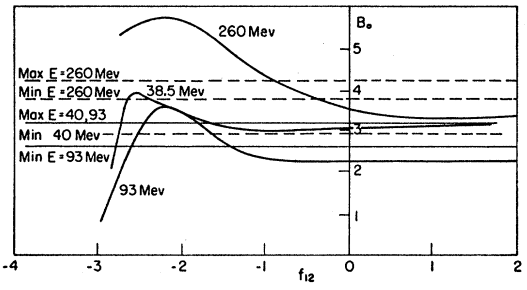

FIG. 6. The coefficient B_0 as a function of f_{12}.

again determined mainly by the ${}^3S_1+{}^3D_1$ states and the isotopic triplet state. Employing the low-energy ${}^3S_1+{}^3D_1$ parameters we plot B_2 in Fig. 7 for 38.5 and 93 Mev. The range $f_{12}>0$ is satisfactory for 93 Mev but proves to be low for 40 Mev. As expected the value of B_2 for $f_{12}>0$ is roughly independent of f_{12} and is therefore determined by the low-energy scattering. Agreement with the experimental value at 40 Mev could be obtained by permitting r_0 for this state to be energy dependent. However, more detailed and precise data in this energy range should be available before such measures are employed. In the calculations to be reported below, we have kept r_0 equal to 1.32×10^{-13} cm for all energies. The parameter f_{12} was placed equal to 1.725, for which f_{10} equals 1.725 and $f_1^{(t)}$ equals (-3.8). The corresponding phase shifts are given in Fig. 2, the coupling coefficient $\epsilon_1^{(1)}$ in Fig. 8.

We may now go on to examine the other coefficients B_L and particularly B_1. One of the principal terms is the interference term between the ${}^3P_2$ and ${}^3S_1+{}^3D_1$ states. The coefficient of the $(1^{(1)}|21)$ term is obtained by multiplying the quantity plotted in Fig. 8 by ten, while the coefficient of the $(1^{(3)}|21)$ term is exactly 10.2 minus the coefficient of the $(1^{(1)}|21)$ term. At the lower energies $\eta_1^{(3)}$ is small, so that nearly the entire interference term is given by the $(1^{(1)}|21)$ term. This is positive, since both phase shifts are positive (the second because of the sign of the $p-p$ polarization) and relatively large because of the large coefficient. The size of the latter is determined by the positive sign of $\epsilon_1^{(1)}$, which in turn is fixed by the sign of the

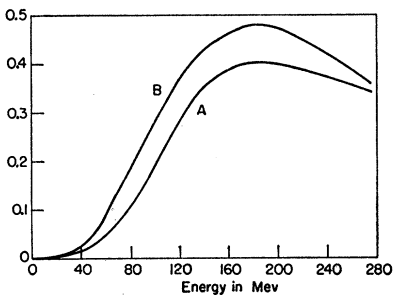

FIG. 5. The coefficient of the $\sin 2\vartheta$ term in Eq. (49) for cases A and B.

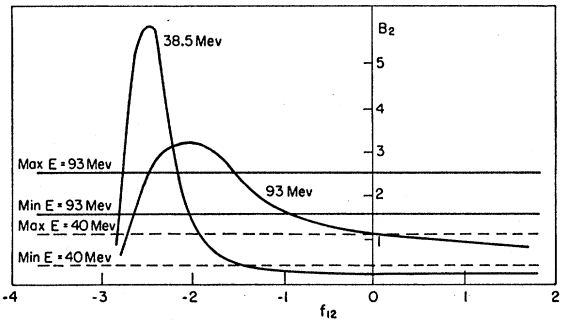

FIG. 7. The coefficient B_2 as a function of f_{12}.

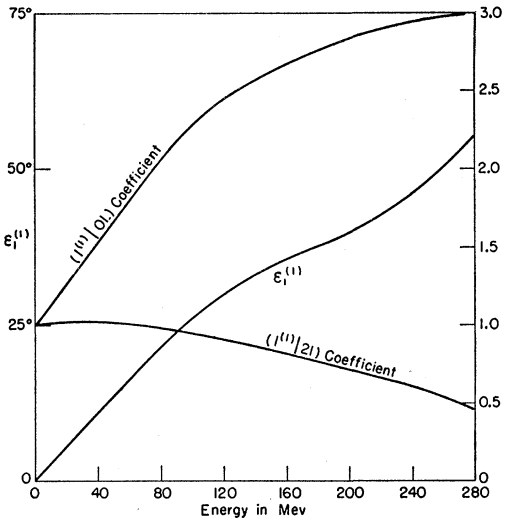

FIG. 8. The coupling angle $\epsilon_1{}^{(1)}$ describing the coupling between the ${}^3S_1$ and ${}^3D_1$ states is given by the left-hand ordinate. The right-hand ordinate measures the coefficient of the $(1^{(1)}|21)$ term divided by 10 and the coefficient of the $(1^{(1)}|01)$ term divided by 2 in B_1.

quadrupole moment. This positive contribution to B_1 decreases with increasing energy. Meanwhile $\eta_1{}^{(3)}$, which is negative, is growing as well as the coefficient of the $(1^{(3)}|21)$ term, so that by 274 Mev the sum of the $(1^{(3)}|21)$ and $(1^{(1)}|21)$ terms is negative. The remaining contributions to B_1 must be chosen negative so as to cancel out the $(1^{(1)}|21)$ contribution at the lower energies and to give a negative excess at the higher energies, in accordance with the experimental data. One may easily verify that this requires η_{01} to be negative, η_{11} to be positive; these were the requirements which dictated our choice of f_{01} and f_{11} in the preceding discussion on $p-p$ scattering. Unfortunately, the negative contribution from η_{01} is not large, principally because the phase shifts η_{01} approach $(-\pi/2)$. In case A, where the phase shift η_0 is always positive, an effective way of obtaining a negative contribution to B_1 is to choose f_1 so that η_1 is negative. Then the contributions of the $(0|1)$ and $(1|2)$ are both negative. These could be made larger if the requirement of isotropy in $p-p$ scattering were relaxed, for then η_2 could be increased.

In case B, η_0 changes sign. However, at low energies only the $(0|1)$ term can be effective, so that again η_1 must be negative and, as may be seen from Fig. 1, will be increasingly negative. Hence, when η_0 changes sign, the $(0|1)$ term will be positive. However, in this case the η_2 phase shifts are considerably larger so that most of this effect is cancelled out by the $(1|2)$ term. The battle to obtain the proper asymmetry for $n-p$ scattering is then taken up in B_3, which must then be negative.

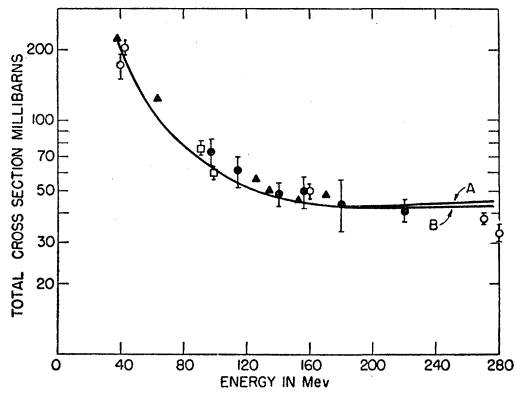

FIG. 9. Total $n-p$ cross section as a function of energy. The unfilled circular points were obtained from Hadley, Kelly, Leith, Segrè, Wiegand, and York [Phys. Rev. **75**, 351 (1949)]; Kelly, Leith, Segrè, and Wiegand [Phys. Rev. **79**, 96 (1950)]; O. Chamberlin and J. W. Easley [Phys. Rev. **94**, 208 (1954)]; J. DeJuren and B. J. Moyer [Phys. Rev. **81**, 919 (1951)]; and R. H. Hildebrand and C. E. Leith [Phys. Rev. **80**, 841 (1950)]. The unfilled square point at 90 Mev is an average of many measurements as given by R. H. Stahl and N. F. Ramsey [Phys. Rev. **96**, 1310 (1954)]. The other square points are from V. Culler and R. W. Waniek [Phys. Rev. **95**, 585 (1954)]. The filled circular points were obtained from Guernsey, Mott, and Nelson [Phys. Rev. **88**, 9 (1952)]. The triangular points are those of Randle, Taylor, Wood, and Snowden[24]; A. E. Taylor and E. Wood [Phil. Mag. **44**, 95 (1953)], and A. E. Taylor [Phys. Rev. **92**, 1071 (1953)].

TABLE III. Angular distribution coefficients B_L. (The coefficient $B_4 \simeq B_4{}^{(1)}$ is given in Table II.)

Energy (Mev)		38.5	80	120	190	274
B_0	A	3.17	2.45	2.39	3.18	4.76
	B	3.16	3.41	2.40	3.13	4.63
B_1	A	−0.17	−0.23	−0.29	−0.35	−0.80
	B	−0.124	−0.051	0.011	0.056	0.402
B_2	A	0.30	0.93	1.52	2.46	4.19
	B	0.30	0.93	1.53	2.47	4.14
	A	0.03	−0.09	−0.21	−0.38	−0.02
	B		−0.21	−0.29	−0.97	−1.09

Here the $(1|2)$ term contributes strongly and also the ${}^3F_3$ terms. This was the main reason for choosing this state to obtain $p-p$ isotropy rather than the ${}^3F_4$ state.

A summary of the results is contained in Table III; the boundary parameters describing the ${}^3S_1+{}^3D_1$ states have already been mentioned. The only additional state added is the ${}^1P_1$, for which, for both the alternatives A and B, the core radius is 1.32×10^{-13} cm and $f_1=2.5$ independent of the energy. We have therefore added only one new parameter beyond the parameters determined by low-energy triplet scattering and $p-p$ scattering and, as shall be seen, we are able to predict the expected neutron-proton scattering fairly well.

Comparison with the data is made in Fig. 9 to Fig. 13. One must bear in mind the wide spread in energy of the neutron beam associated with each nominal experimental neutron energy. Excellent agreement with the data is obtained for the total cross section Q_{np} and $\sigma_{np}(90°)$, the latter being not too well known. From the other figures it is clear that the cross sections at 0° and 180° are considerably less than the experimental values. The angular distributions at 90 and 300 Mev are duplicated fairly well but do not rise high enough

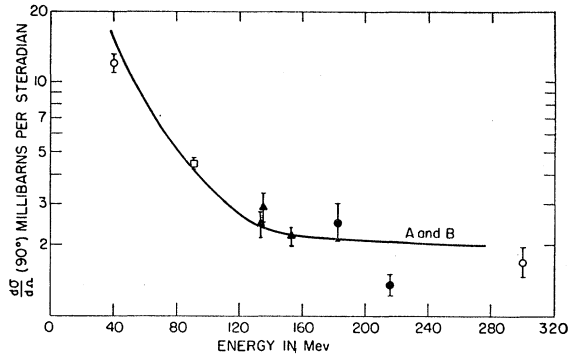

FIG. 10. Differential $n-p$ cross section at 90° in the center-of-mass system as a function of neutron laboratory energy. The unfilled circular points are taken from J. Hadley *et al.* [Phys. Rev. **75**, 351 (1949)], and J. de Pangher [Phys. Rev. **95**, 578 (1954)]. The unfilled square point is that of R. H. Stahl and N. F. Ramsey [Phys. Rev. **96**, 1310 (1954)]. The triangular points are those of Thresher, Voss, and Wilson [Proc. Roy. Soc. (London) **A229**, 402 (1955)]. Randle, Taylor, and Wood [Proc. Roy. Soc. (London) **A213**, 213 (1952)]. Randle, Cassels, Pickavance, and Taylor [Phil. Mag. **44**, 425 (1953)] and Randle and Uridge (unpublished). The filled circular points are from Guernsey, Mott, and Nelson [Phys. Rev. **88**, 15 (1952)].

at 180° for both cases and at 0° for 90 Mev. We shall defer discussion of possible remedies to the Conclusions.

V. CONCLUSIONS

We have found that the boundary-condition approximation is simple to use and provides a broad correlation of the experimental data. We have been able to fit in most particulars the existing scattering data up to 274 Mev employing only one energy-dependent parameter, the core radius r_0 for the $^1S_0$ state. The boundary parameters employed are given in Tables IV and V. The chief omission has been the angular dependence of the $p-p$ polarization data. We have assumed this to have the simple form $\sin 2\vartheta$.

Two principal features of the fit which are probably model-independent are

(a) The $p-p$ scattering is composed mostly of scattering in the $^1S_0$ and $^3P_0$ states. The scattering from the latter is close to the scattering by a repulsive sphere of radius 1.32×10^{-13} cm.

(b) The scattering in the isotopic singlet state below 100 Mev, assuming that the angular distribution is symmetric about 90°, is determined entirely by the $(^3S_1+^3D_1)$ states. The scattering in this state up to 100 Mev is predicted from the fit of the triplet scattering data near zero neutron energy. Above 100 Mev, the $(^3S_1+^3D_1)$ states still make the major contribution, although a considerable effect must come from other states; in our fit from the $^1P_1$ state.

One methodological result noted is that the fit of proton-proton data and that of the neutron-proton data must be considered together. The odd terms in the $n-p$ angular distribution depend critically upon the interference between the isotopic triplet and isotopic singlet states. In the present paper this determined the sign of the $^3P_0$ phase shift and the type of states included in achieving isotropy for $p-p$ scattering.

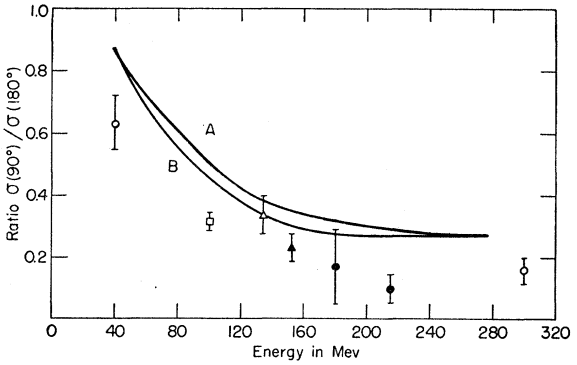

FIG. 11. Ratio of the differential $n-p$ cross section at 90° to that of 180° in the center-of-mass system as a function of neutron laboratory energy. References are the same as those in Fig. 10.

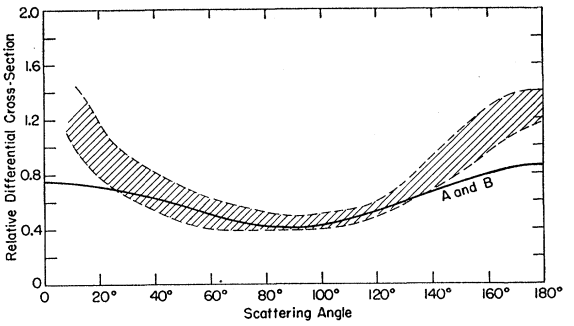

FIG. 12. Relative differential $n-p$ cross section at 90 Mev. The shaded area represents the available experimental data as given by R. H. Stahl and N. F. Ramsey [Phys. Rev. **96**, 1310 (1954)]. The theoretical curve is adjusted to agree with experiment at 90°. For comparison of experimental and theoretical normalization see Fig. 9.

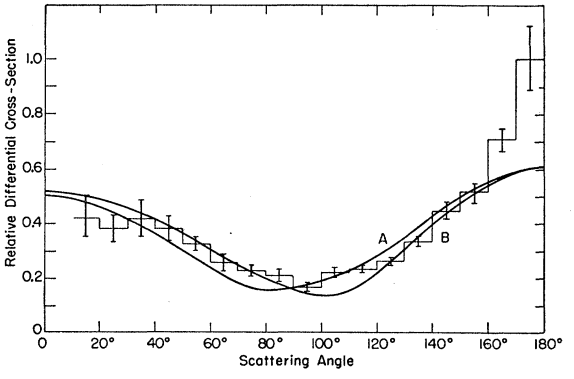

FIG. 13. Relative differential $n-p$ cross section at 300 Mev. The experimental points are those of J. de Pangher [Phys. Rev. **95**, 578 (1954)]. J. W. Easley [University of California Radiation Laboratory Report UCRL-2693 (unpublished)] has obtained small angle points which are some 20% higher than those of dePangher. These would agree very closely with the theoretical curve. The theoretical curve is adjusted to agree with experiment at 90°. For comparison of experimental and theoretical normalizations, see Fig. 9.

TABLE IV. Boundary parameters for the isotopic triplet states. States for which no entries were made were assumed to give negligible contributions to the scattering. The parameter $f_2^{(t)}$ was placed equal to zero. Energies E are expressed in Mev in the laboratory system. A and B refer to the two types of fit attempted.

State		$^1S_0$	$^1D_2$	$^3P_0$	$^3P_1$	$^3P_2$	$^3F_2$	$^3F_3$
r_0 (10^{-13} cm)	A	$1.32e^{-0.03\sqrt{E}}$	1.32	1.32	0.88	0.88		
	B	$1.32e^{-0.02\sqrt{E}}$	1.32	1.32		1.1	1.32	1.32
f_J	A	−0.947	1.0	−16	0.45	0		
	B	−0.947	0.6	−16		0		1.5

We note also the type of data which appears most useful. In $p-p$ scattering the polarization experiments, the sign and angular distribution are most important. It would also be valuable if measurements of the degree of isotropy in $p-p$ scattering similar to that at Harvard[19] at 90 Mev and California[20] at 300 Mev were made at other energies. In $n-p$ scattering, more detailed information on the angular distributions are needed, particularly the cross section at 0° and 180°. It would be undoubtedly worth while to obtain much of this detailed information in the lower energy range where fewer states enter in the scattering.

The chief failure in the fit reported here is in the cross section at 180° in $n-p$ scattering. A good fit is predicted in the range 30° to 120°, but outside of this range the predicted cross sections fall below the experimental ones. This is not too surprising inasmuch as one would expect the model to fail for these close encounters. This comparison could be improved considerably if the $p-p$ scattering is more anisotropic than we allowed, or if the ratios $\sigma_{np}(0°)/\sigma_{np}(180°)$ are considerably larger at the higher energies than present experiments indicate. Otherwise, it would be necessary to make other parameters energy dependent. For example, the $^3P_0$ state could be required to contribute less strongly at the higher energies, and the $^3P_1$ more strongly. Further information on these states should become available soon upon completion of phase shift analyses being performed at Yale and California. Note that we have also omitted the effects of meson production which may be of some importance at the higher energies. It would be expected that such effects be still fairly small at 274 Mev, but that they should tend to help explain the observed forward-to-back ratio.

TABLE V. Boundary parameters for the isotopic singlet states.

State	$^3S_1+^3D_1$	$^1P_1$
r_0 (10^{-13} cm)	1.32	1.32
	$f_{01}=1.72=f_{12}$ $f_1^{(t)}=-3.80$	$f_1=2.5$

An earlier attempt by us[28] to fit the data by using the boundary-condition approximation should be mentioned here. A common energy-independent core radius was employed for all states. The reactance matrix could then be expressed in terms of spin, orbital angular momentum and isotopic spin operators. Considerably fewer parameters than those given on Table IV were required to obtain a fair fit. This attempt failed, however, in that it predicted the wrong sign for the polarization at 240 Mev although the magnitude of the polarization was correct.

ACKNOWLEDGMENTS

The authors are greatly indebted to Professor Julian Schwinger, Professor Victor Weisskopf, and Dr. R. Raphael for many helpful suggestions. They are indebted to Professor R. Wilson for a very helpful discussion of the experimental data. One of us (H.F.) did a major part of this work while on educational leave of absence from the Massachusetts Institute of Technology as a Guggenheim fellow. He would like to take this opportunity to thank the Physics Department at Harvard University for their hospitality during this period. The other (E.L.) was a holder of the Quebec Postgraduate Fellowship and the E.I. du Pont de Nemours Fellowship.

[28] Earle Lomon, Massachusetts Institute of Technology thesis, 1954 (unpublished).

Note added in proof.—Since this paper was written, the $p-p$ scattering experiments at 300 Mev at California have been analyzed by Dr. Henry Stapp. His results are in qualitative agreement with our results for Case B, but are not in good quantitative agreement.